

Theoretical Study of Spin-dependent Electron Transport in Atomic Fe Nanocontacts

Hugh Dalgleish and George Kirczenow

Department of Physics, Simon Fraser University, Burnaby, British Columbia, Canada V5A 1S6

(Dated: August 14, 2018)

We present theoretical predictions of spintronic transport phenomena that should be observable in ferromagnetic Fe nanocontacts bridged by chains of Fe atoms. We develop appropriate model Hamiltonians based on semi-empirical considerations and the known electronic structure of bulk Fe derived from *ab initio* density functional calculations. Our model is shown to provide a satisfactory description of the surface properties of Fe nano-clusters as well as bulk properties. Lippmann-Schwinger and Green's function techniques are used together with Landauer theory to predict the current, magneto-resistance, and spin polarization of the current in Fe nanocontacts bridged by atomic chains under applied bias. Unusual device characteristics are predicted including negative magneto-resistance and spin polarization of the current, as well as spin polarization of the current for anti-parallel magnetization of the Fe nanocontacts under moderate applied bias. We explore the effects that stretching the atomic chain has on the magneto-resistance and spin polarization and predict a cross-over regime in which the spin polarization of the current for parallel magnetization of the contacts switches from negative to positive. We find resonant transmission due to dangling bond formation on tip atoms as the chain is stretched through its breaking point to play an important role in spin-dependent transport in this regime. The physical mechanisms underlying the predicted phenomena are discussed.

PACS numbers: 75.47.-m,73.63.-b,72.25.-b,72.10.-d

I. INTRODUCTION

Spin-dependent transport (SDT) phenomena occur when a bias voltage is applied across a junction between materials one or both of which are magnetic.¹ They include partial or complete spin-polarization of the electric current and changes in the electrical resistance when the magnetization direction of one of the magnetic components of the system is reversed through the application of a magnetic field. The latter effect is usually referred to as “junction magneto-resistance” or “giant magneto-resistance” (GMR). SDT has been observed at interfaces between ferromagnetic metals and superconductors², between ferromagnetic and normal metals³, between ferromagnetic metals separated by thin insulating films⁴, and more recently between magnetic semiconductors and nonmagnetic semiconductors.^{5,6}

At the present time spin-dependent transport through nanoscale junctions is attracting increasing attention. SDT through molecules bridging nanoscale magnetic contacts has been investigated theoretically^{7,8,9,10} and relevant experiments have recently been reported.^{11,12,13,14} SDT through chains of atoms or single atoms connecting pairs of nickel and cobalt nanocontacts has also been investigated theoretically.^{15,16,17,18,19} Such systems have been realized experimentally using break-junction^{20,21,22,23,24} and electrochemical²⁵ techniques and transport measurements on them have been carried out.^{20,21,22,23,24,25} SDT measurements have also been carried out on Fe atomic contacts and magnetoresistances an order of magnitude smaller than for the Ni and Co systems were found.²⁶ This difference was explained in terms of the smaller ratio between the spin *up* and spin *down* densities of states at the Fermi level in bulk Fe than in Ni

or Co.²⁶ Very recently, a theoretical study elucidating the systematics of SDT through a variety of nanocontacts, including Fe nanocontacts connected by atomic chains, has been reported.¹⁶ The calculations were based on a semi-empirical tight-binding model and were carried out in the limiting case of infinitesimal applied bias voltage. The structures studied were periodic arrays of nanoconstrictions with all of the Fe atoms occupying sites of a bulk crystal lattice and enough vacant sites being included in the structure to isolate the Fe chains from each other.

In this article we explore SDT through Fe atomic chains connecting Fe nanocontacts theoretically in some important regimes that were not considered in the previous work: We develop a model applicable to more general atomic geometries; thus we are able to examine the effects on SDT of stretching the atomic chain that bridges the Fe nanocontacts as occurs in break-junction experiments. We predict pronounced resonant spin-dependent transport phenomena due to dangling bonds that form on the tip atoms as the atomic chain parts. We also consider the application of finite bias across the junction of the Fe nanocontacts and predict other unusual SDT phenomena including negative junction magneto-resistance and negative spin-polarization of the current. We define these quantities as follows:

The junction magneto-resistance (JMR) is defined as

$$JMR = \frac{(I_{par} - I_{anti})}{\frac{1}{2}(I_{par} + I_{anti})} \quad (1)$$

where I_{par} (I_{anti}) is the electric current flowing between the Fe nanocontacts when their magnetizations are parallel (antiparallel).

The spin-polarization of the current (SP) is defined as

$$SP = \frac{(I_{up} - I_{down})}{\frac{1}{2}(I_{up} + I_{down})}. \quad (2)$$

Note that we refer to the majority spins in *each* contact as “spin *up*” and the minority spins as “spin *down*”. Thus if an electron is transmitted between contacts with anti-parallel magnetizations without changing its spin orientation, the transition will be referred to as a spin *up* \rightarrow spin *down* or spin *down* \rightarrow spin *up* transition. In equation (2) I_{up} (I_{down}) is the spin *up* (spin *down*) current with *up* and *down* defined as for the nanocontact that is the electron *drain* electrode for the system. The total current is defined as $I = I_{up} + I_{down}$ for both parallel and antiparallel magnetizations.

We find that, interestingly, in equation (2) the current for the spin with the larger bulk density of states is not always larger than the current for the spin with the smaller density of states. Thus the sign of the spin polarization of the current cannot be predicted from a knowledge of the spin *up* and *down* densities of states alone, even when the magnetizations of the two nanocontacts are parallel. We also show that the spin polarization of the current need not vanish even for the case of anti-parallel magnetizations of the two nanocontacts because of a symmetry breaking that occurs in the system under finite applied bias. Furthermore we predict that the sign of the the junction magnetoresistance should change when the atomic chain connecting the nanocontacts is stretched and also if the applied bias voltage is increased sufficiently.

Our SDT calculations are based on Landauer theory²⁷ and Lippmann-Schwinger and Green’s function techniques. Transport calculations require a knowledge of the underlying electronic structure. Semi-empirical tight-binding models of electronic structure have been used successfully in modeling SDT in thin film structures involving Fe and other magnetic metals together with insulating or vacuum tunnel barriers or non-magnetic metal spacers,^{28,29,30,31,32} and also SDT in magnetic metal nanocontacts.¹⁶ They have also been used successfully to explain the experimental current-voltage characteristics of molecular nanowires connecting non-magnetic metal electrodes.^{33,34,35} In this paper, we model the Fe nanocontacts as nanoclusters of Fe atoms connected to ideal leads that represent the source and drain electrodes. However we parameterize the electronic structure of the Fe clusters with the use of semi-empirical tight-binding parameters obtained from fitting the known band structure of magnetic bulk Fe.³⁶ Never-the-less, as we explain in Section II, our model also provides a satisfactory description of the spin-resolved surface densities of states and of the local magnetic moments at the surfaces of Fe nanoclusters. Thus our model incorporates in an approximate way *both* the bulk and surface magnetic properties of Fe which together influence the SDT through a junction of bulk Fe leads that come together at a nanocontact, as in experimental realizations of Fe atomic chains.

This article is organized as follows: In Section II we describe our model of the geometry and electronic and magnetic structure of the Fe nanocontacts. In Section III we summarize the formalism used in our spin-dependent transport calculations. In Section IV this formalism is applied to different arrangements of Fe atoms connecting the ferromagnetic nanoclusters: We start by considering a structure in which the positions of the atoms of the Fe nanocontacts and of the atomic bridge connecting them coincide with sites of an Fe crystal, however we consider a single atomic bridge, as distinct from the periodic array of nanocontacts treated in Ref. 16. The spin-dependent currents flowing through this junction are calculated utilizing initially a simple, voltage-independent model of the transmission probabilities of spin *up* and spin *down* electrons through the junction. A strong magneto-resistance is predicted. We then perform voltage-dependent calculations of the transmission to examine the effects of finite bias on the spin-dependent predictions more closely and obtain a still strong, though relatively weaker, JMR. We then proceed to examine geometries in which the separation of nanoclusters is allowed to vary, stretching the atomic chain. To this end, we supplement the above tight-binding model of the electronic structure of the Fe clusters³⁶ by introducing a position-dependent parameterization for the electronic coupling between clusters, in the spirit of extended-Hückel theory. We allow the separation between the tips of the clusters to range from a bulk nearest-neighbor distance, in which case ballistic SDT is predicted, to a distance at which the atomic chain has been broken and vacuum-tunneling-like SDT occurs. The cross-over regime is examined and interesting phenomena are predicted, including spin-dependent transport resonances mediated by dangling bonds on the tip atoms. In the ballistic regime, unusual device characteristics such as negative JMR and spin polarization of the current are predicted. We then proceed to apply our approach to the case of tunneling between ferromagnetic nanoscale tips separated by vacuum and examine the spin-dependent current and magneto-resistance. Physical mechanisms are presented that explain the predicted effects. The $I - V$ characteristics and magneto-resistance predictions presented in this paper should be experimentally accessible. Our conclusions are summarized in Section V.

II. THE MODEL

The system of interest consists of two bulk ferromagnetic metal electrodes that act as a source and drain for electrons, joined by a nanoscale junction of atoms of the same magnetic metal. We model this structure as a connected pair of nanoscale contacts of (100) body-centered cubic iron, each contact consisting of a 55 atom cluster built from 5x5, 4x4, 3x3, 2x2 layers of atoms, terminated with a single tip atom. Thus the atomic chain bridging the nanocontacts is a dimer consisting of the two tip Fe

atoms.

The electronic structure of the Fe clusters is described by a tight-binding Hamiltonian using a non-orthogonal basis of s , p and d atomic orbitals, a total of 9 orbitals per atom for each spin orientation. The values of the Hamiltonian matrix elements $H_{i,j}$ and overlaps $S_{i,j} = \langle i|j \rangle$ between orbitals i and j are, where possible, taken from Ref. 36. These tight-binding parameters are based on fits to *ab initio* band structures calculated for Fe crystals³⁶ and have previously been employed successfully to study magnetic multilayer systems²⁹ and magnetic¹⁶ and non-magnetic³⁷ atomic chain nanoscale systems. However this parameter set is modified and/or extended appropriately (as discussed below and in Sections IV A and IV B 1, respectively) when a magnetic domain wall is present or a finite bias voltage is applied across the junction or the positions of the atoms of the junction do not all coincide with sites of a perfect bcc Fe crystal lattice.

The source and drain electrodes are modeled as sets of one-dimensional ideal leads coupled to each cluster. These ideal leads are implemented as semi-infinite tight-binding chains with one orbital per site, one such lead being coupled to each (s, p and d , spin *up* and spin *down*) orbital of each atom of the two layers of each Fe cluster that are furthest from the junction. The site-orbital energy of each ideal lead is matched to that of the Fe tight binding orbital to which the lead couples and the lead band widths are chosen large enough that all of the eigenstates of the leads are propagating modes in the energy range of interest. As well as mimicking macroscopic electrodes by supplying an ample electron flux to the system, this large number of ideal source and drain leads (369 per cluster for each spin orientation) has an effect similar to phase-randomizing Büttiker probes³⁸ in minimizing the influence of dimensional resonances due to the finite sizes of the Fe clusters employed in the model. Thus our results do not change qualitatively if the parameters of the ideal leads are varied (within reasonable bounds) or an additional layer of Fe atoms is included in the clusters.

We assume that each cluster (including the tip atom) and the semi-infinite leads connected to it form a single magnetic domain. Thus, if the magnetizations of the two nanocontacts are anti-parallel, an atomically thin, hard domain wall is present at the midpoint of the Fe dimer connecting the two clusters, in accordance with the calculation of Ref. 39 and with previous work modeling SDT in Ni atomic contacts.¹⁸ The tight-binding parameters developed in Ref. 36 do not include the off-diagonal Hamiltonian or overlap matrix elements between atomic orbitals located on opposite sides of a magnetic domain wall. However the published off-diagonal matrix elements connecting spin *up* orbitals are not very different from the corresponding matrix elements connecting spin *down* orbitals in the same domain.³⁶ This is physically reasonable given the that spatial part of a spin *up* orbital should be similar to that of the corresponding spin *down* orbital. Thus in the present work, at zero bias, when geometrically applicable, we approximate the off-diagonal matrix

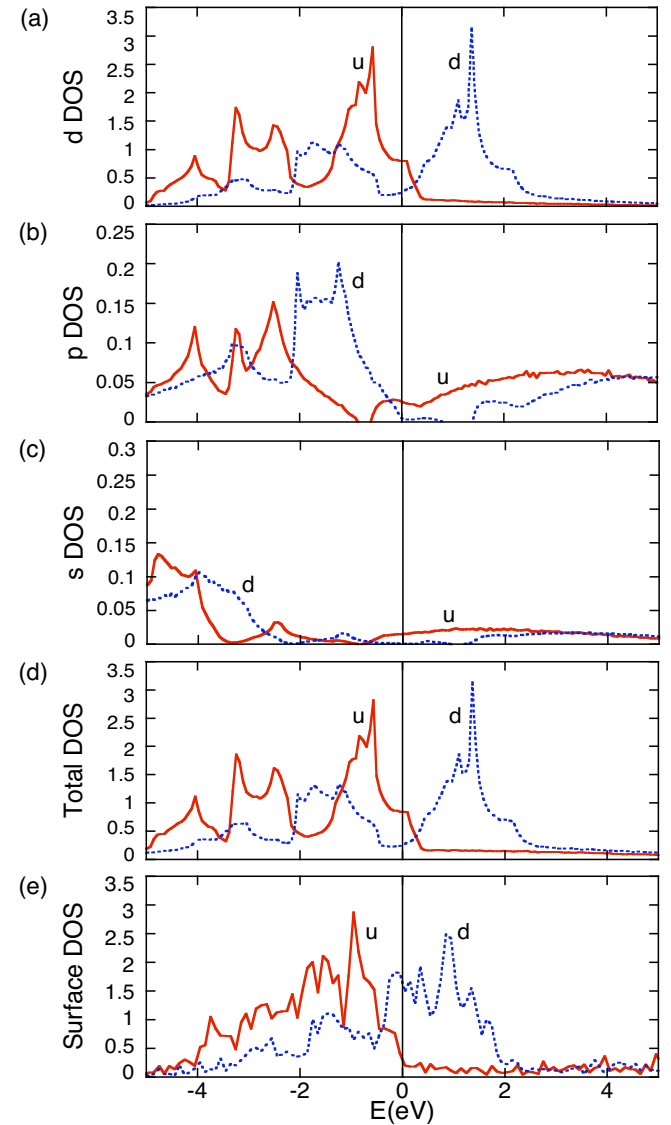


FIG. 1: (Color online) Calculated bulk (a-d) and surface (e) densities of states vs. energy (eV) at zero bias for spin *up* (solid curve *u*) and spin *down* (dotted curve *d*). The Fermi energy is located at 0 eV. (a) The densities of states due to *d*-electrons. (b) The densities of states due to *p*-electrons. (d) The densities of states due to *s*-electrons. (d) The total densities of states. The *d* orbital contribution dominates the total density of states except at the higher and lowest energies shown. (e) The surface contribution to the densities of states.

elements connecting orbitals that are on *opposite* sides of an atomically thin domain wall and have the *same* spin orientation by the average of the spin *up* and spin *down* matrix elements connecting the corresponding orbitals in a single domain. As in Ref. 36, we also take all Hamiltonian and overlap matrix elements connecting orbitals having opposite spin orientations to be zero, i.e., spin flips during electron transmission through the junction are not considered.

To better understand the significance of the results of

our SDT calculations it will be useful to compare them to particular features of the spin-resolved surface and bulk densities of states of the Fe electrodes and to further resolve the density of states into its *s*, *p* and *d* components. Since the atomic orbital basis that we use is non-orthogonal we carry out this resolution as follows: Consider the normalized eigenstate $|\Psi_k\rangle = \sum_i c_{k,i} |i\rangle$ of the Hamiltonian, where $|i\rangle$ is an atomic orbital. Express the norm of the eigenstate in terms of the contributions of all of the atomic orbitals of the system as

$$\langle \Psi_k | \Psi_k \rangle = \sum_{i,j} c_{k,i}^* c_{k,j} S_{i,j} \quad (3)$$

where $S_{i,j} = \langle i|j\rangle$. To resolve the contribution of eigenstate $|\Psi_k\rangle$ to the density of states into its *s*, *p* and *d* orbital components we assign to each atomic orbital *i* the Mulliken weight $c_{k,i}^* c_{k,i} + \sum_{j \neq i} (c_{k,i}^* c_{k,j} S_{i,j} + c_{k,j}^* c_{k,i} S_{j,i})/2$. The partial and total bulk densities of states obtained in this way are shown in Fig. 1 (a-d).

In order to assess the applicability of our semi-empirical tight binding model (that is based on fits to bulk band structures³⁶) to nanostructures that include surfaces, we calculated the local magnetic moment per atom in the surface atomic layer and in the interior of each of several large Fe clusters. A similar Mulliken analysis to that described above was used to resolve the electron probability distributions for individual eigenstates of the tight-binding Hamiltonian used in the present work into surface and interior contributions. We found the lower coordination number and lack of symmetry at the surface to result in enhanced magnetic moments at the surface, approximately $2.5\mu_B$ per atom at the surface versus $2.2\mu_B$ in the bulk for our model, a result qualitatively similar to that of *ab initio* surface calculations for Fe (2.25 in the bulk and 2.98 at the surface).⁴⁰ We note that Mulliken analyses arbitrarily assign half of the probability contribution that is due to overlaps between two atoms in equation (3) to each of the two atoms involved and therefore tend to underestimate differences between the electronic populations of adjacent atoms, often significantly. Thus we regard the level of agreement between the present model and the *ab initio* surface calculations⁴⁰ as satisfactory. The contributions from the surface layer of a representative Fe cluster to spin *up* and spin *down* densities of states obtained in this way are shown in Figure 1(e) and compare well with those reported in Ref. 40.

As further indication that our semi-empirical model is appropriate for describing also the nanocontact region (the two tip atoms) in addition to the rest of the contacts approximating bulk electrodes, we have employed the model to predict magnetic moments of *actual* Fe nanoclusters of increasing size. The results of this calculation are compared to those of *ab initio* calculations on identical nanoclusters⁴¹ in Figure 2(a-d). It is evident that the predicted moments of our semi-empirical model compare well to those of the *ab initio* study for both the surface and interior atoms of the clusters, particularly when

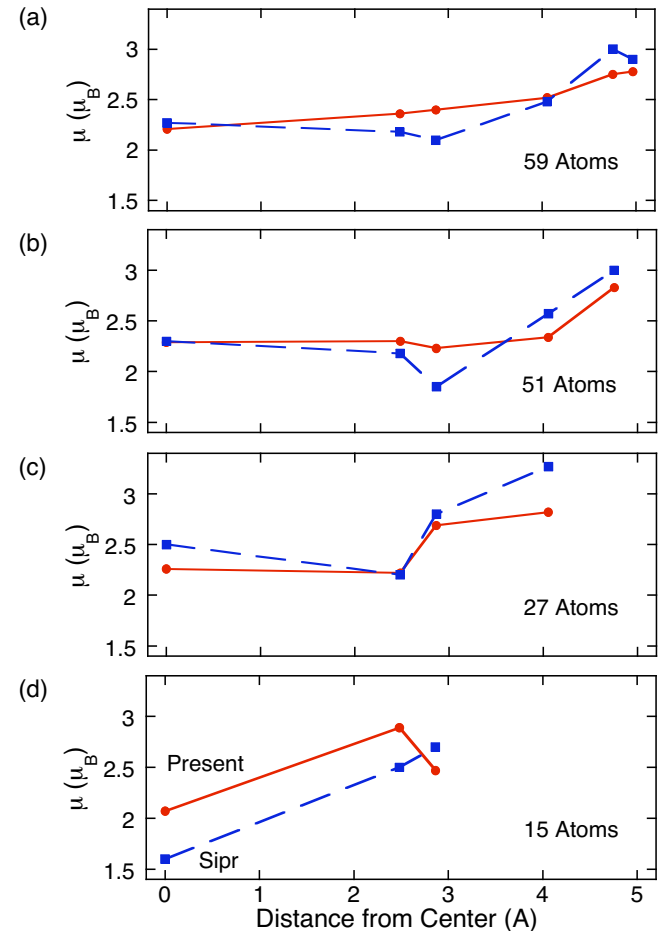


FIG. 2: (Color online) Calculated magnetic moments per atom as a function of atom distance relative to the central atom of Fe nanoclusters. Solid lines correspond to the present study, dashed lines to the first principles calculations of Šipr *et al.*⁴¹ All atoms are at bulk lattice positions and cluster size is increased as additional coordination shells are added. (a) 15 atom Fe cluster. (b) 27 atom cluster. (c) 51 atom cluster. (d) 59 atom cluster.

the cluster size resembles that of our nanoclusters used for the transport calculation (51 and 59 atom clusters compared to the 55 atom clusters we employ in our following study). We consider the good agreement for the outermost atoms of the clusters as indication that our model adequately reproduces the magnetic properties of even atoms of low coordination number, such as the tip atoms of the clusters in our transport calculations. Additionally, as the nanocluster size is increased (to the 51 and 59 atom sized clusters), the magnetic moments of all of the interior atoms quickly approach that of the bulk. Therefore these results also provide further evidence that the Fe clusters employed in our transport calculations are large enough to model macroscopic magnetic Fe electrodes (with single atom tips) if our semi-empirical tight binding model is used to treat the electronic and magnetic structures of these systems.

III. THEORY OF SPIN-DEPENDENT TRANSPORT

When a bias V is applied between the ferromagnetic Fe electrodes an electric current I flows through the nanoscale junction described in Section II. Landauer theory²⁷ relates this current to the multi-channel probability T for an electron to scatter from the source electrode to the drain via the junction, according to

$$I(V) = \frac{e}{h} \int dE T(E, V) [f(E, \mu_S) - f(E, \mu_D)] \quad (4)$$

where E is the energy of the electron, $F(E, \mu)$ is the equilibrium Fermi distribution and $\mu_{S,D} = E_F \pm eV/2$ are the electro-chemical potentials of the source (S) and drain (D) electrodes in terms of the common Fermi energy, E_F .⁴² The transmission probability in equation (4) is

$$T(E, V) = \sum_{\alpha, \beta, s, s'} \left| \frac{\nu_{\beta, s'}}{\nu_{\alpha, s}} \right| |t_{\beta, s'; \alpha, s}|^2 \quad (5)$$

where $t_{\beta, s'; \alpha, s}$ is the transmission amplitude from a state of ideal lead α of the source electrode with spin s to a state of ideal lead β of the drain electrode with spin s' and $\nu_{\alpha, s}$ and $\nu_{\beta, s'}$ are the corresponding electron velocities. If spin flips during transmission of electrons through the junction are neglected as in the present work and the summations over spin in equation (5) for T are restricted to a particular spin orientation then equation (4) yields the current for that spin orientation, i.e., I_{up} or I_{down} .

We calculate T numerically by solving the Lippmann-Schwinger equation⁴³

$$|\Psi^\alpha\rangle = |\Phi_0^\alpha\rangle + G_0(E)W|\Psi^\alpha\rangle \quad (6)$$

where $G_0(E)$ is the Green's function for the system with the coupling W between the ideal leads and Fe clusters switched off, $|\Phi_0^\alpha\rangle$ is the eigenstate of ideal lead α when it is decoupled from the Fe clusters, and $|\Psi^\alpha\rangle$ is the corresponding eigenstate of the complete system with coupling W switched on. The transmission amplitudes $t_{\beta, s'; \alpha, s}$ that appear in equation (5) are obtained from the solution $|\Psi^\alpha\rangle$ of the Lippmann-Schwinger equation (6).

IV. RESULTS

A. Fe Nanocontacts Bridged by Fe Atoms in a bcc Nearest-Neighbor Geometry

We begin by considering the nanocontact geometry shown in the inset of Figure 3(a). Here the two 55 atom clusters are placed so that the atom terminating the tip of each cluster is at a bulk nearest neighbor position relative to the tip atom of the other cluster. Thus all atoms occupy positions that match sites of a body-centered cubic Fe bulk lattice so that a tight-binding Hamiltonian

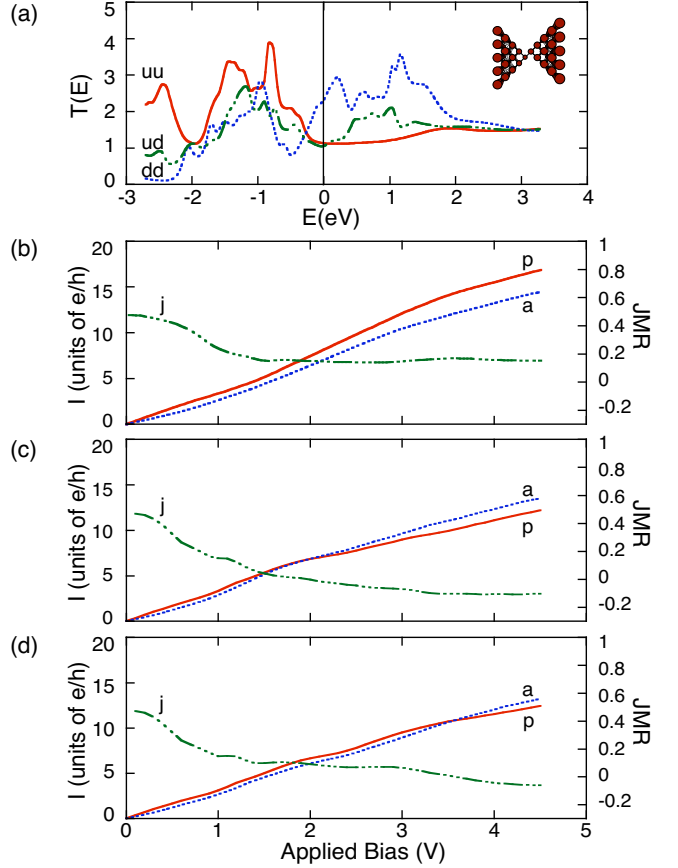


FIG. 3: (Color online) (a) Transmission probabilities as a function of energy (eV) at zero bias for the contact geometry shown in the inset where all of the atoms are located at sites of a bulk Fe bcc lattice. Spin $up \rightarrow up$ (uu), $down \rightarrow down$ (dd) transmission probabilities are for parallel magnetization of the two contacts; $up \rightarrow down$ (ud) is for anti-parallel magnetization. The Fermi energy is located at 0eV. (b) The current as a function of voltage for parallel (p) and anti-parallel (a) magnetizations calculated by integrating the zero bias transmission probabilities in (a). The JMR (j) is also shown. (c) The currents and JMR as calculated with an applied bias using the linear voltage drop model. (d) The currents and JMR as calculated with an applied bias using the abrupt voltage drop model.

and overlap matrix for the entire structure can be constructed using the parameter set of Ref. 36. Figure 3(a) shows the calculated transmission probabilities for the different spin configurations, at zero bias, for this geometry. The spin $up \rightarrow up$ (uu) and $down \rightarrow down$ (dd) transmission probabilities are for parallel magnetization of the two contacts; $up \rightarrow down$ (ud) is for anti-parallel magnetization. The Fermi energy is at 0eV. The transmission characteristics depend somewhat on the specific details of the chosen geometry, such as cluster size and shape. However, quite similar results are obtained when a 6x6 atom layer is added to each of the clusters. Current and magneto-resistance results are also robust to geometrical changes, such as addition of a 6x6 layer, or

deletion of the 5x5 layer that terminates the nanocluster, indicating that the clusters and ideal leads in our model adequately represent real (macroscopic) Fe leads.

For this geometry, the calculated spin *up* \rightarrow *up* transmission, perhaps surprisingly for a transition metal, exhibits a fairly flat plateau close to unity near and above the Fermi energy. As for atomic chains constructed from some non-magnetic metals³⁷, this transmission near unity in the spin *up* case is not due to a single open conducting channel, but to the superposition of partially conducting channels. By systematically switching off the tip atom-to-tip atom coupling for different atomic orbital symmetries, we deduce that the *up* \rightarrow *up* transmission near the Fermi energy is due primarily to *s* and *p* electrons, even though as is seen in Figure 1 the spin *up* density of states due to *d* electrons is comparable to those due to *s* and *p* electrons above the Fermi energy. Below the Fermi energy, the bulk and surface densities of states for *up* electrons are larger (primarily *d*-like), and the predicted transmission is also higher.

In contrast to the spin *up* case, the spin *down* \rightarrow *down* transmission near the Fermi energy, not only shows a strong contribution from *p*-type electrons but a very strong *d*-electron component; *s*-electrons do not seem important in this case. This also can be contrasted to the spin *down* densities of states very near the Fermi energy where that due to *p*-electrons is small and comparable to that for *s*-electrons. Yet the presence of many common features that can be observed in the calculated transmission and the surface and bulk densities of states does support the conclusion that the spin transport properties of this magnetic system are influenced by the densities of states. However, the transmission characteristics can not be determined from solely a knowledge of the densities of states; characteristics such as the near quantum conductance above the Fermi energy in the spin *up* channel and the magnitudes of the transmission features can not be deduced from the densities of states alone. Those characteristics can be determined only from a full quantum transport calculation such as that presented here.

Interestingly, as shown in Figure 3(a), the calculated spin *down* \rightarrow *down* transmission is significantly larger than the spin *up* \rightarrow *up* transmission near the Fermi energy and thus according to equations (2) and (4) our theory predicts a negative spin polarization of the current through this junction at low bias for parallel magnetization of the two contacts. Negative spin polarization of the current is a common feature of theories that attempt to estimate spin-dependent transport effects in Ni and Co heterostructures simply from convolutions of the spin-dependent densities of states of the magnetic electrodes that are dominated by the contributions of *d* electrons. However, such approximations have been shown incorrect in magnetic tunnel junctions, as *d*-electron wave functions decay very quickly in the insulating barrier^{2,29,30,31,45,46}. This decay is further enhanced by the conservation of wavevector parallel to the interface^{45,47}, and therefore the *d*-electrons that are

responsible for the strongest features in the densities of states do not play an active role in transmission in such insulator mediated systems. In atomic chain systems however, there is no lateral periodicity, and parallel wavevector conservation is broken. Also, the magnetic electrodes that we consider are in this case in physical contact and so *d*-electrons do play an active role in transport⁴⁸. Never-the-less, a convolution of the bulk densities of states cannot account for the negative spin polarization of the current that we predict in the present system; it arises from a combination of effects due to the surface and bulk densities of states *and* our full quantum mechanical treatment of electron transmission through the junction.

The transmission probability $T(E, V)$ that enters the Landauer expression (4) for the electric current I flowing through the nanocontact depends on the applied bias voltage V as well as the electron energy. The bias dependence of T depends on the potential profile through the nanocontact which is difficult to calculate from first principles since this is a non-equilibrium many-body property. However, appropriate heuristic models for the profile can yield accurate results for the current.⁴⁹ We adopt this approach here by comparing the results obtained for a variety of simple models.

Figure 3(b) shows the current calculated by approximating $T(E, V)$ with $T(E, 0)$, an approximation commonly used to study transport at low values of the bias. Here, and in all of the figures and discussion that follow, the current refers to the flow of electrons, or electron flux, as electrons are transported from the source to the drain electrode. In Figure 3(b) the calculated current is higher for parallel magnetization than for anti-parallel magnetization and steadily increases with applied bias, characteristic of ballistic transmission. The calculated JMR, as defined by Eq. 1 is positive and larger at low bias, decaying to a lower value of about 0.15 at high bias.

Figure 3(c) and (d) show our results obtained using explicitly bias-dependent transmission probabilities $T(E, V)$ that were calculated for two different models of the potential profile of the nanocontact. In each case we assume that the entire voltage drop occurs across the narrowest constriction in the system, i.e. over the dimer. Thus all atoms (and ideal leads) to the source side of the dimer are assumed to be at a potential $\phi = -\frac{V}{2}$, while atoms and leads to the drain side are at $+\frac{V}{2}$. For the results shown in Figure 3(c) the potential is assumed to vary linearly through the region occupied by the dimer.^{49,50,51,52,53} In Figure 3(d), for comparison, the potential is assumed to change abruptly from $\phi = \pm\frac{V}{2}$ in the atomic layers adjacent to the dimer to $\phi = 0$ on the two atoms that constitute the dimer itself, a profile analogous to that proposed initially in theoretical work on ballistic semiconductor nanostructures⁵⁴ and more recently adopted in modeling certain molecular wires.^{51,55}

In each case the electrostatic potential modifies the diagonal matrix elements of the tight-binding Hamiltonian of the system which become $H_{i,i} = H_{i,i}^0 - e\phi_i$ where $H_{i,j}^0$

is the tight-binding Hamiltonian matrix at zero bias and ϕ_i is the electrostatic potential ϕ at the site occupied by atomic orbital i . Because the tight binding basis that we use is non-orthogonal, the applied electrostatic potential also modifies the non-diagonal Hamiltonian matrix elements.⁵⁶ Here we include this effect approximately in the form

$$H_{i,j} = H_{i,j}^0 - eS_{i,j}(\phi_i + \phi_j)/2. \quad (7)$$

The applied electrostatic potential breaks the symmetry between the left and right clusters in the inset in Figure 3(a). Symmetry breaking often results in weaker transmission probabilities in quantum transport, and this has qualitative implications for the present system: The symmetry breaking as energy levels are shifted apart manifests itself in a somewhat lower transmission and current for parallel magnetization of the contacts (especially at higher bias) in Figure 3(c) and (d) than in Figure 3(a) where the effect of the applied bias on the transmission is neglected. However the net current for anti-parallel magnetization is much less sensitive to bias-related symmetry effects.⁵⁷ Because it selectively depresses the current for parallel magnetization of the contacts, the bias-induced symmetry breaking results in a crossover with increasing bias from positive to negative values of the JMR in Figure 3(c) and (d), an effect not found in the less realistic model of Figure 3(a) where the effect of the bias on the electron transmission probability is neglected.

The bias voltage at which we predict negative JMR to appear ($\sim 2V$ in Figure 3(c) and $\sim 3.5V$ in Figure 3(d)) depends on the details of the potential profile across the junction where the two electrodes touch: In the linear voltage drop model the bias applied across the junction *simultaneously* shifts the energies of similar atomic orbitals on the two tip atoms, bringing them closer together or further apart, depending on their relative spin orientations and whether the magnetizations of the contacts are parallel or antiparallel. Thus orbitals of the tip atoms are brought closer to or further from resonance with each other. On the other hand, since in the abrupt voltage drop model the applied bias affects the energies of all of the atomic orbitals of the contacts *except* those of the tip atoms, the corresponding resonant effect of the applied bias in this model is weaker: energies of orbitals within a cluster are shifted with respect to *unshifted* energy levels on the tip atoms (the energy levels of the rest of the clusters are not directly coupled to any other atoms in the opposing cluster). Therefore, the onset of negative JMR requires a higher applied bias in the abrupt voltage drop model.

B. Spin-Dependent Transport for More General Junction Geometries

It has been established experimentally that the conductance characteristics of atomic chains can be altered

by stretching them⁵⁸. We now investigate the corresponding dependence of the JMR in our magnetic system.

1. Generalizing the Tight-Binding Model

For the more general junction geometries, our Hamiltonian matrix elements between atomic orbitals within each of the two Fe clusters will again be based, as discussed above, on the Fe ferromagnetic tight-binding parameters derived from *ab initio* bulk band structure calculations³⁶. However a different approach is needed to obtain the non-diagonal Hamiltonian matrix elements that describe tip-to-tip coupling since the atoms involved no longer all fall on sites of a single bcc Fe lattice. We estimate these matrix elements using an appropriate modification of extended Hückel theory. Extended Hückel⁵⁹ is a semi-empirical tight-binding model from quantum chemistry that provides a simple description of the electronic structures of a wide variety of molecules. It uses a non-orthogonal atomic orbital basis. The diagonal Hamiltonian matrix elements $H_{i,i}$ are identified with the experimental ionization energies of the corresponding atomic orbitals i of isolated atoms. In the Wolfsberg-Helmholtz form of the model⁶⁰ the non-diagonal matrix elements are assumed to be

$$H_{i,j} = \frac{K}{2}(H_{i,i} + H_{j,j})S_{i,j} \quad (8)$$

where $S_{i,j}$ are the overlap matrix elements connecting orbitals i and j that are calculated by approximating the atomic orbitals i and j with linear combinations of Slater-type orbitals. K is a phenomenological parameter, usually chosen to be 1.75, in order to match experimental data. We estimate the non-diagonal Hamiltonian matrix elements that describe tip-to-tip coupling using equation (8) and numerical values of the diagonal Hamiltonian matrix elements based on those given in Ref. 36. However, the values of the diagonal matrix elements given in Ref. 36 are not close to the ionization energies of the corresponding atomic orbitals but are defined up to an arbitrary additive constant. It is necessary to choose the value of this constant with care in order to obtain realistic results from equation (8). We choose its value so that when the two tips are positioned in the geometry studied in Section IV A, our model (including the tip-to-tip coupling matrix elements obtained using equation (8)) reproduces the *up* \rightarrow *up* transmission near the Fermi energy obtained using only the bulk parameters from Ref. 36. The value of the shift that we apply to the bulk electronic parameters is $c = -13.53\text{eV}$.⁶¹ The same tip-to-tip coupling parameters $H_{m,n}$ are then used for all spin configurations.⁶² This is consistent with the fact that bulk *up-up* coupling parameters are very similar to *down-down* parameters³⁶.

Thus in our calculations the overlaps $S_{i,j}$ between Slater-type orbitals provide the *distance and orientation-dependence* of the tip-to-tip Hamiltonian matrix elements

required for the more general junction geometries (as in extended Hückel theory), however, the Hamiltonian matrix elements are normalized so as to yield transport results consistent with those obtained from a Hamiltonian matrix derived from *ab initio* calculations.

2. Structural Considerations: Bulk and Relaxed Geometries

The first geometry we consider using this hybrid model is shown in the inset of Figure 4(a). The two (100) 5x5, 4x4, 3x3, 2x2, and single tip atom clusters are now aligned with a common axis. The two tip atoms are again separated by a bulk nearest neighbor distance, 2.482Å. We refer to this as the “linear geometry,” and to the structure in the inset of Figure 3(a) as the “skewed geometry.” Our geometry relaxations⁶³ on simple model systems involving the pair of 2x2 planes and the two atoms forming the dimer, indicate that the two tip atoms in this geometry are close to their stable positions. Similar relaxations that we carried out showed that when the clusters are pulled apart, some stretching occurs between the tip atoms and their respective 2x2 layers, but most of the stretching occurs between the two tip atoms. When the tips are far apart representing vacuum tunneling, our geometry relaxations show that, with respect to the rest of the cluster, the tip atom sits very near its bulk position. Therefore, we assume that as the junction is stretched, all of the stretching occurs between the two tip atoms, and so the atoms of each tip separately are located on their bulk Fe lattice positions. Therefore, in what follows, we again make use the bulk Fe ferromagnetic tight-binding parameters to describe the electronic structure within the clusters for all matrix elements in H , and use our modified Hückel approach to describe the inter-cluster coupling.⁶⁴

3. SDT in Fe Nanocontacts Bridged by Fe Atoms in Contact in a Linear Geometry

Our results for spin transport in the linear geometry with the tip atoms separated by a bulk nearest neighbor distance are shown in Figure 4. The spin *up* \rightarrow *up* transmission shown in Figure 4(a) shows a similar plateau above E_F to that in the skewed geometry (Figure 3(a)). This similarity is due to the dominance of the non-directional *s*-orbitals in both cases. Below the Fermi energy, the transmissions exhibit significant differences, due to the importance of the very directional *d*-orbitals in that energy range. For the two different geometries, spin *down* \rightarrow *down* and *up* \rightarrow *down* transmissions are similar in a broad sense, such as overall magnitude, but display many differences on a finer scale due to the importance of *d* orbitals in those transmissions. Figure 4(b) shows that the current through this geometry, as calculated from the voltage-independent transmissions, is smaller than that through the skewed geometry using bulk parameters to

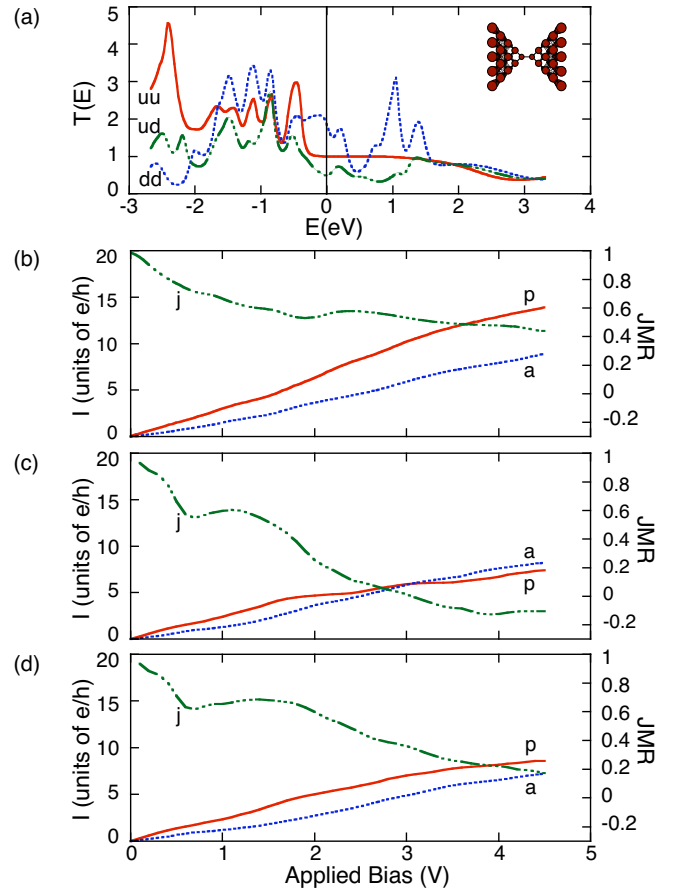


FIG. 4: (Color online) (a) The transmission probabilities as a function of energy (eV) at zero bias for the spin *up* \rightarrow *up* (*uu*), *down* \rightarrow *down* (*dd*), and *up* \rightarrow *down* (*ud*) configurations for the Fe atoms at the nearest neighbor separation, arranged in the linear geometry (inset). The Fermi energy is located at 0eV. (b) The current as a function of voltage for parallel (*p*) and anti-parallel (*a*) magnetizations in the zero bias approximation for the transmission probabilities. The JMR (*j*) is also shown. (c) The currents and JMR as calculated with an applied bias using the linear voltage drop model. (d) The currents and JMR as calculated with an applied bias using the abrupt voltage drop model.

describe the coupling. However, with second nearest-neighbor couplings across the junction turned off in the skewed geometry, the current in the parallel magnetization configuration is in very close agreement for the two geometries suggesting that the lower current can be attributed to the lack of second nearest neighbor coupling between the two contacts in the linear geometry. In the anti-parallel magnetization configuration, the current is substantially lower in the linear geometry than in the skewed geometry. This reflects the lower spin *up* \rightarrow *down* transmission in the the linear geometry which results partly from weaker *d* coupling: Many of the overlaps involving *d* orbitals are zero in the linear geometry. The substantially lower anti-parallel current results in a significantly stronger JMR.

As shown in Figure 4(c) the current for parallel magnetization and the magneto-resistance, as calculated from the voltage-dependent transmission in the linear voltage drop model, are again significantly lower than for the voltage-independent transmission model for the linear geometry (at higher bias) because the Hamiltonian is no longer symmetric. The current is slightly weaker for the linear geometry than for the skewed geometry and a larger JMR is predicted than for the skewed geometry. A negative JMR is again predicted, but this time it manifests near a bias of 3V. As was discussed for the skewed geometry, in the linear voltage drop model the applied bias *simultaneously* moves the atomic orbitals of the tip atoms closer or further apart in energy. Thus the linear voltage drop model provides a relatively strong mechanism for those energy levels to move closer to or further from resonance with each other. However, in the present case of the linear geometry, there is no second neighbor coupling between a tip atom and atoms of the opposite contact and so the resonant effect is weaker than in the previous case of the skewed geometry. The potential profile with abrupt voltage drops is also less conducive to negative JMR here (as in the skewed geometry) thus a negative JMR does not occur within the voltage range in Figure 4(d). It should also be noted that the predictions regarding $I - V$ characteristics and JMR in the two geometries are qualitatively similar for the linear voltage drop model which, according to density functional calculations,⁴⁹ may be a more accurate approximation for all-metal systems than the abrupt voltage drop model. However, the predicted results are qualitatively similar for *both* models of the potential profile in both systems, demonstrating the robustness of our method; it is reasonable to expect the results of a fully self-consistent calculation of the potential profile to fall between these two model profiles. Again, all of these results are also reasonably robust to the addition of a 6x6 atom layer to each of the clusters.

4. Dependence of the Spin Transport on the Separation Between Tip Atoms and Dangling Bond Formation

Figure 5(a-c) shows the calculated dependence of the magnetoresistance and spin polarization of the current (as defined by Eqs. (1) and (2), respectively) on the separation between the two tip atoms as the junction is stretched for two values (0.5 and 1.0V) of the bias voltage, for the linear voltage drop model.

As the separation between tip atoms is increased, the JMR (Figure 5(a)) initially decreases rapidly then increases to a local maximum at tip separations near 3.5 and 4Å then resumes its decrease turning weakly negative and, for the 0.5V bias, increases again at large separations. The spin polarization of the current for parallel magnetization of the contacts (Figure 5(b)) is negative at small separations, i.e., the spin *down* (minority spin) current predominates, and rises initially with increasing

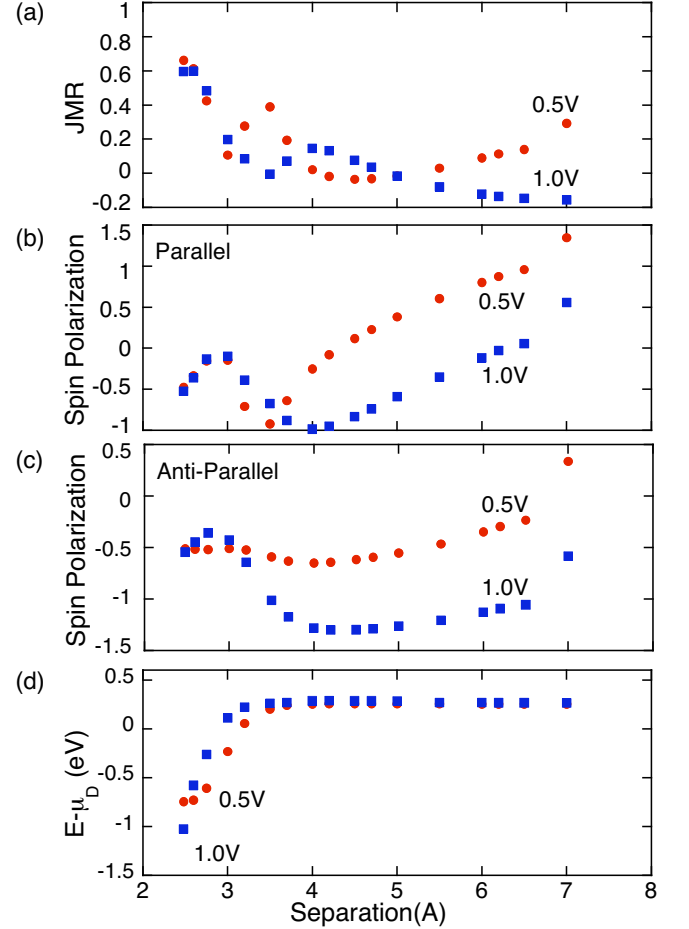


FIG. 5: (Color online) Spin dependent transport in the linear tip geometry vs. separation of the tip atoms. (a) The JMR as a function of tip separation calculated using the linear voltage drop model and applied biases of 0.5V and 1.0V. (b) The spin polarization of the current as a function of tip separation for parallel magnetization of the contacts. (c) The spin polarization of the current as a function of tip separation for anti-parallel contact magnetizations. (d) The energy eigenvalue associated with the spin *down* dangling bond state relative to the chemical potential of the drain electrode (0eV) as a function of tip separation for parallel magnetization of the contacts.

separation almost to zero near 3Å. It then passes through a minimum near 3.5 and 4Å (where the JMR shows a maximum) before resuming its rise and becoming positive at large separations. The local maxima in the JMR and minima in the spin polarization of the current near 3.5 and 4Å are due to a pronounced resonance in the dominant *down* \rightarrow *down* transmission that appears near the Fermi energy for parallel magnetization of the contacts at such separations. This transmission resonance persists when a 6x6 Fe layer is added to each nanocontact, thus it does not appear to be a dimensional resonance due to the finite size of our Fe clusters.

By examining the contributions of the individual electronic eigenstates of the Hamiltonian of the coupled Fe

clusters to the *down* \rightarrow *down* transmission (through the Green's function G_0 in the Lippmann-Schwinger equation (6)) we have identified the particular eigenstate that is responsible for this transmission resonance. Our Mulliken analysis revealed that for tip separations corresponding to the appearance of the *down* \rightarrow *down* transmission resonance, a significant portion of this eigenstate resides on the tip atom of the drain contact⁶⁵ and has $d(x^2 - y^2)$ orbital symmetry there; the $d(x^2 - y^2)$ orbital has a lobe oriented along the x -axis towards the tip atom on the other cluster. Since the $d(x^2 - y^2)$ orbital is involved in tip-to-tip bonding and the amplitude of the eigenstate of interest on the tip atom increases as the tip separation is increased, we attribute the appearance of this eigenstate state to bond-breaking between the tip atoms and the associated formation of a dangling bond.

The energy E of the dangling bond eigenstate relative to the electrochemical potential of the drain is plotted in Figure 5(d) as a function of tip separation for the two values of applied bias considered in Fig. 5(a-c). The dangling bond state is the dominant feature in the Mulliken spectra of the tip atom within a broad window about the Fermi energy and this criterion is used to identify the state for the different values of the tip separation and applied bias. At zero temperature, only states within the limits of integration corresponding to the applied bias contribute to the predicted current (see Eq. 4). These limits are determined by the electrochemical potentials of the source (0.5eV and 1.0eV in Figure 5(d) for the two values of applied bias) and the drain (0eV). As shown in the figure, as the tip separation is increased, the energy of the dangling bond state shifts into the window of integration, above the electrochemical potential of the drain and therefore begins to contribute to the current. (Note that this happens at separations close to those where the JMR in Fig.5(a) first begins to rise signaling the onset of the transport resonance). Simultaneously, the Mulliken weight of the state located on the drain tip increases as the separation is increased to a value of about 10 percent, a sizeable portion of the total probability distribution of the eigenstate given that a total of 110 atoms make up the Fe clusters in our model. Therefore, as the separation is increased from its smallest distance of 2.482Å, we attribute the initial decrease in JMR to the stretching of the bond between the two tip atoms. The following increase to the local maximum in JMR is attributed to the formation of a dangling bond as the tips are further pulled apart, leading to the resonant feature in the *down* \rightarrow *down* transmission. Once the dangling bond has been formed, its energy and Mulliken weight are roughly constant, and the JMR resumes its decrease with increasing separation.

As was discussed in Section IV A, *s*, *p* and *d* electrons all play a significant role in transport in this system for small tip separations. However their contributions decay differently as the tip separation is increased and the tunneling regime is entered. Since the valence *d*-electrons have a lower site energy than the other electrons

($E_d < E_s, E_p$),³⁶ they decay more rapidly resulting in a less significant contribution from *d*-electrons to transport as the tip separation is increased.

For an applied bias of 0.5V and near a tip separation of about 4.5Å, the contribution to tunneling from *d*-electrons is roughly equal to that of *s*-electrons. Here $T_{up \rightarrow up}$, mostly due to *s*-electrons, and $T_{down \rightarrow down}$, mostly due to *d*-electrons, are roughly equal and the spin polarization of the current in the parallel magnetization case (Fig. 5 (b)) is roughly zero, defining a cross-over regime. This can be viewed as the cross-over from ballistic transmission to a tunneling-like transport. At the cross-over, transmission from spin *up* (mostly *s* and *p*) to spin *down* (mostly *d*) for antiparallel magnetization of the contacts is roughly the same as that for the parallel spin configurations, and the resulting JMR (Fig. 5 (a), 0.5V) is very small, or even slightly negative. Since this small negative magneto-resistance appears at a relatively small applied bias, it should be accessible experimentally in these systems.

At larger separations, beyond the cross-over regime, the current is dominated by the transport of *s* and *p* electrons and $T_{up \rightarrow up}$ makes the largest contribution. Therefore the spin polarization of the current in the parallel magnetization case (Fig. 5 (b)) is positive, and growing. Since transmission involving *down* (mostly *d*) electrons is rapidly decreasing, $T_{down \rightarrow down}$ and $T_{up \rightarrow down}$ are small (due to band mismatch the anti-parallel transmission in general is smaller than even the decreasing *down* \rightarrow *down* transmission) and, as can be seen in Fig.5 (a) in the 0.5V case, the JMR also begins to slowly grow. At higher biases (for example at 1.0V bias in Fig.5(a) and (b)) more energy levels are sampled, increasing the importance of the *d* states and the cross-over doesn't occur until larger separations. Therefore, this model predicts that when *d* states are important, the current will be dominated by minority electrons, and when *d* states are negligible, current due to majority electrons will dominate. This is quite analogous to the predictions made by Mathon on periodic systems involving Co and tunneling gaps of varying widths, where the fast decrease in *d*-electron transport accounts for a rapid reversal in sign of the spin-polarization³⁰.

Since the application of bias breaks the symmetry of the Hamiltonian, $T_{up \rightarrow down} \neq T_{down \rightarrow up}$ and a non-zero spin polarization of the current is predicted in the anti-parallel magnetization case as well. This effect is entirely due the voltage drop across the junction and so is expected to be unique to magnetic transport systems that can sustain a significant potential drop across the junction, i.e, atomic nanocontacts and tunnel junctions. As shown in Figure 5(c), the spin polarization of the current for antiparallel magnetization of the contacts (as defined by Eq. 2) is negative over a wide range of tip separations due to the dominance of the *up* \rightarrow *down* transmission under applied bias as a result of shifting energy levels. Even at relatively low bias, there is more source and drain energy level overlap in this configura-

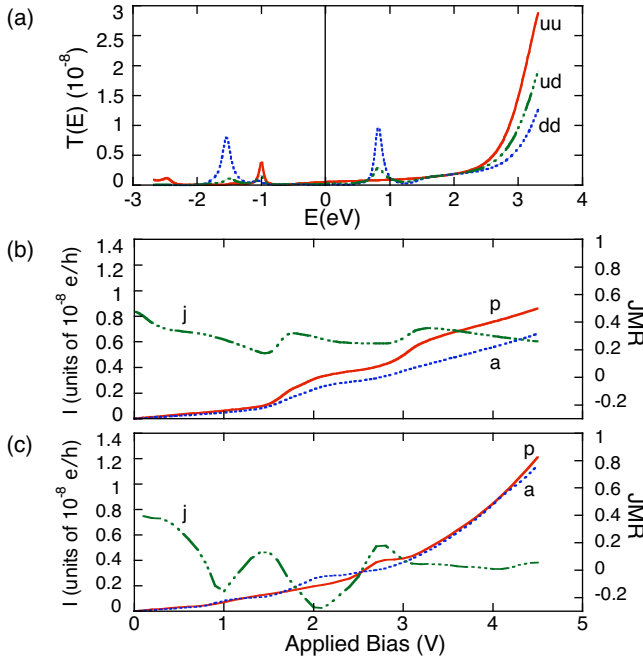


FIG. 6: (Color online) (a) The transmission probabilities as a function of energy (eV) at zero bias for the spin $up \rightarrow up$ (uu), $down \rightarrow down$ (dd), and $up \rightarrow down$ (ud) configurations for a 7Å tip separation representative of the vacuum tunneling regime. The Fermi energy is located at 0eV. (b) The current as a function of voltage for parallel (p) and anti-parallel (a) magnetizations as calculated by integrating the zero bias transmission probabilities in (a). The JMR (j) is also shown. (c) The currents and JMR as calculated with an applied bias using the linear voltage drop model.

tion than in the $down \rightarrow up$ configuration where levels are shifted apart by the applied bias. At higher bias, this is even more the case, resulting in a much more negative spin polarization of the current at 1.0V. Never-the-less, the spin polarization does increase for large tip separations as the d -state transport becomes less significant. The non-monotonic behavior of the spin polarization of the current with tip separation for separations below 4Å in Fig.5(c) is due to resonant transport associated with dangling bond formation similar to that for the case of parallel magnetization of the contacts that is discussed in detail above.

5. Vacuum Tunneling Between Fe Nanocontacts

When the separation between tip atoms is very large (vacuum tunneling), the d -electron states have decayed across the gap between the contacts and do not significantly contribute to the transmission. This situation is easier to analyze as the couplings between tip atoms involving s and p_x (all the rest are negligible) behave simply. Figure 6(a) shows the calculated transmission for the linear geometry with a tip atom separation of

7Å at zero bias. The currents calculated using the zero bias approximation for T , shown in Figure 6(b), display step-like features due to peaks in the transmission. The zero-bias approximation for T also predicts a strong JMR effect, which shows broad peaks where the transmission resonances are encountered.

Figure 6(c) shows the $I - V$ characteristics calculated using the linear voltage drop model for $T(E, V)$. The application of bias and shifting of energy levels strongly damps the local maxima in the zero bias transmissions and the step-like behavior seen in Figure 6(b) is now less pronounced. The current increases with bias, resembling the accepted behavior of tunneling through vacuum. At the application of about 2V, the $up \rightarrow down$ transmission becomes the strongest scattering channel, so the anti-parallel current becomes stronger than the parallel current. This results in a relatively strong, negative JMR, although the $down \rightarrow down$ transmission regains its dominance and positive JMR returns at higher bias. Thus the shifting of different transmission maxima again results in non-monotonic behavior of the JMR and negative JMR for some values of the applied bias. However, there is no sustained JMR reversal such as is predicted when d -electron states contribute to transport.

V. CONCLUSIONS

We have presented a microscopic quantum theory of spin-dependent transport across iron nanoscale junctions bridged by chains of Fe atoms, based on the Landauer approach to transport, semi-empirical tight-binding Hamiltonians and Lippmann-Schwinger and Green's function scattering techniques. We first applied bulk ferromagnetic tight-binding parameters (that were shown to also provide a satisfactory description of surface properties) to study ballistic transport between a pair of Fe contacts connected by two Fe atoms in a nearest neighbor geometry. We presented theoretical predictions for the current-voltage characteristics of this system for parallel and anti-parallel magnetizations of the contacts and predicted that negative spin polarization of the current should occur at low bias. We also predicted that the junction magnetoresistance of this system should switch sign from positive to negative with increasing bias. Next, we extended our model so as to allow us to study spin-dependent transport for more general tip geometries and presented predictions of the junction magnetoresistance and spin polarization of the electric current through Fe nanoscale junctions as a function of separation between the tip atoms of the nanocontacts from nearest neighbor distances to the vacuum tunneling regime. Characteristic trends emerging in those transport predictions as the separation is varied were associated with decay rates of different orbitals and with the breaking of bonds and associated dangling bond formation resulting in spin-dependent transmission resonances. We also presented a systematic physical interpretation of our predictions that

in many cases are qualitatively different from those that rely on density of states considerations alone, and also different from the behavior of SDT in thin film junctions where lattice periodicity in directions orthogonal to that of the current flow plays a key role. Many of our predictions apply in the regime of low bias that should be accessible with present day experimental techniques.

Acknowledgments

We thank B. Heinrich, R. Hill and B. L. Johnson for helpful discussions. This research was supported by NSERC and the Canadian Institute for Advanced Research.

¹ For reviews of the literature see
 S.A. Wolf, D.D. Awschalom, R.A. Buhrman, J.M. Daughton, S. von Molnar, M. L. Roukes, A. Y. Chtchelkina, D. M. Treger, *Science* **294**, 1488 (2001);
 I. Zutic, J. Fabian, S. Das Sarma, *Rev. Mod. Phys.* **76**, 323 (2004).

² R. Meservey, P. M. Tedrow, and P. Fulde, *Phys. Rev. Lett.* **25**, 1270 (1970).

³ M. Johnson and R. H. Silsbee, *Phys. Rev. Lett.* **55**, 1790 (1985).

⁴ M. Julliére, *Phys. Lett.* **54A**, 225 (1975).

⁵ R. Fiederling, M. Keim, G. Reuscher, W. Ossau, G. Schmidt, A. Waag, and L. Molenkamp, *Nature (London)* **402**, 787 (1999).

⁶ Y. Ohno, D. K. Young, B. Beschoten, F. Matsukura, H. Ohno, and D. D. Awschalom, *Nature (London)* **402**, 790 (1999).

⁷ E. G. Emberly, G. Kirczenow, *Chem. Phys.* **281**, 311 (2002).

⁸ R. Pati, L. Senapati, P. M. Ajayan, and S. K. Nayak, *Phys. Rev. B* **68**, 100407(R) (2003).

⁹ W. I. Babiacyk and B. R. Bulka, *J. Phys.: Cond. Matt.* **16**, 4001 (2004).

¹⁰ A. R. Rocha, V. M. García-Suárez, S. W. Bailey, C. J. Lambert, J. Ferrer, and S. Sanvito, *Nature Materials* **4**, 335 (2005).

¹¹ V. Dediú, M. Murgia, F. C. Matacotta, C. Taliani, and S. Barbanera, *Solid State Commun.* **122**, 181 (2002).

¹² Z. H. Xiong, D. Wu, Z. V. Vardeny, J. Shi, *Nature* **427**, 821 (2004).

¹³ J. R. Petta, S. K. Slater, and D. C. Ralph, *Phys. Rev. Lett.* **93**, 136601 (2004).

¹⁴ D. Wu, Z. H. Xiong, X. G. Li, Z. V. Vardeny and J. Shi, *Phys. Rev. Lett.* **95**, 016802 (2005).

¹⁵ G. Tatara, Y. -W. Zhao, M. Muñoz, and N. Garcia, *Phys. Rev. Lett.* **83**, 2030 (1999).

¹⁶ J. Velev and W. H. Butler, *Phys. Rev. B* **69**, 094425 (2004).

¹⁷ A. Bagrets, N. Papanikolaou, and I. Mertig, *Phys. Rev. B* **70**, 064410 (2004).

¹⁸ J. J. Palacios, D. Jacob, J. Fernández-Rossier, *cond-mat/0406249* (2004).

¹⁹ A. R. Rocha and S. Sanvito, *Phys. Rev. B* **70**, 094406 (2004).

²⁰ H. Oshima and K. Miyano, *Appl. Phys. Lett.* **73**, 2203 (1998).

²¹ N. Garcia, M. Muñoz, and Y.-W. Zhao, *Phys. Rev. Lett.* **82**, 2923 (1999).

²² T. Ono, Y. Ooka, and H. Miyajima, Y. Otani, *Appl. Phys. Lett.* **75**, 1622 (1999).

²³ M. Viret, S. Berger, M. Gabureac, F. Ott, D. Olligs, I. Petej, J. F. Gregg, C. Fermon, G. Francinet, and G. Le Goff, *Phys. Rev. B* **66**, 220401 (2002); M. Gabureac, M. Viret, F. Ott, and C. Fermon, *Phys. Rev. B* **69**, 100401 (2004).

²⁴ C. Untiedt, D. M. T. Dekker, D. Djukic, and J. M. van Ruitenbeek, *Phys. Rev. B* **69**, 081401 (2004).

²⁵ M. R. Sullivan, D. A. Boehm, D. A. Ateya, S. Z. Hua, H. D. Chopra, *cond-mat/0404348* (2004).

²⁶ N. Garcia, M. Muñoz, and Y. -W. Zhao, *Appl. Phys. Lett.* **76**, 2586 (2000).

²⁷ For a review see S. Datta, *Electronic Transport in Mesoscopic Systems*, Cambridge University Press, Cambridge, 1995.

²⁸ E. Yu Tsymbal and D. G. Pettifor, *J. Phys.: Cond. Matt.* **9**, L411 (1997).

²⁹ J. Mathon and A. Umerski, *Phys. Rev. B* **63**, 220403(R) (2001).

³⁰ J. Mathon, *J. Phys. D: Appl. Phys.* **35**, 2437 (2002).

³¹ J. Mathon, *Phys. Rev. B* **56**, 11810 (1997).

³² J. Mathon, A. Umerski, and M. Villeret, *Phys. Rev. B* **55**, 14378 (1997).

³³ S. Datta and W. Tian, S. Hong and R. Reifenberger, J. I. Henderson and C. P. Kubiak, *Phys. Rev. Lett.* **79** 2530 (1997).

³⁴ E. Emberly and G. Kirczenow, *Phys. Rev. Lett.* **87**, 269701 (2001), *Phys. Rev. B* **64**, 235412 (2001).

³⁵ J. G. Kushmerick, D. B. Holt, J. C. Yang, J. Naciri, M. H. Moore, R. Shashidhar, *Phys. Rev. Lett.* **89**, 086802 (2002).

³⁶ D. A. Papaconstantopoulos, *Handbook of the Band Structure of Elemental Solids*, Plenum Press, New York, 1986.

³⁷ J. C. Cuevas, A. Levy Yeyati, and A. Martín-Rodero, *Phys. Rev. Letters.* **80**, 1066 (1997); A. Levy Yeyati, A. Martín-Rodero and F. Flores, *Phys. Rev. B* **56**, 10369 (1997).

³⁸ M. Büttiker, *Phys. Rev. B* **33**, 3020 (1986).

³⁹ P. Bruno, *Phys. Rev. Lett.* **83**, 2425 (1999).

⁴⁰ S. Ohnishi and A. J. Freeman, M. Weinert, *Phys. Rev. B* **28**, 6741 (1983).

⁴¹ O. Šípr, M. Kosuth and H. Ebert, *Phys. Rev. B* **70**, 174423 (2004).

⁴² The calculations presented here were carried out for zero temperature.

⁴³ Since the tight-binding atomic orbital basis we use is non-orthogonal, we follow the methodology described in Ref.44.

⁴⁴ E. G. Emberly and G. Kirczenow, *Phys. Rev. Lett.* **81**, 5205 (1998); E. G. Emberly and G. Kirczenow, *Journal of Physics Condensed Matter* **11**, 6911 (1999).

⁴⁵ W. H. Butler, X. -G. Zhang, and T. C. Schultness, J. M. MacLaren, *Phys. Rev. B* **63**, 054416 (2001); X. -G. Zhang and W. H. Butler, *J. Phys.: Cond. Matt.* **15**, R1603 (2003).

⁴⁶ E. Y. Tsymbal, O. N. Mryasov, and P. R. LeClair, *J. Phys.: Cond. Matt.* , R109 (2003).

⁴⁷ J. M. MacLaren, X. -G. Zhang, W. H. Butler, *Phys. Rev. B* **56**, 11827 (1997).

⁴⁸ We note that Garcia *et al.*²⁶ have interpreted experimental data in terms of *d*-state transport in Fe atomic chains.

⁴⁹ S.-H. Ke, H. U. Baranger, and W.T. Yang, Phys. Rev. B **70**, 085410 (2004).

⁵⁰ P. L. Pernas, A. Martín-Rodero, and F. Flores, Phys. Rev. B **41**, 8553 (1990).

⁵¹ V. Mulica, A. E. Roitberg, M. Ratner, J. Chem. Phys. **112**, 6834 (2000).

⁵² P. S. Damle, A. W. Ghosh, and S. Datta, Phys. Rev. B **64**, 201403 (2001).

⁵³ S. Pleutin, H. Grabert, G. Ingold, and A. Nitzan, cond-mat/0209091 (2002).

⁵⁴ L. I. Glazman and A. V. Khaetskii, Europhys. Lett. **9**, 263 (1989).

⁵⁵ E. G. Emberly and G. Kirczenow, Phys. Rev. B **58**, 10911 (1998).

⁵⁶ See Ref. 7, Appendix A.

⁵⁷ For anti-parallel magnetization of the contacts the applied bias brings the spin *up* orbitals of the source contact into resonance with similar spin *down* orbitals of the drain contact, resulting in increased symmetry between the two contacts and therefore the *up* \rightarrow *down* transmission increases with increasing bias. However, no such resonant effect occurs for *down* \rightarrow *up* transmission which decreases with increasing bias. Thus the effect of the applied bias on the *total* transmission for anti-parallel magnetization is relatively small.

⁵⁸ G. Rubio, N. Agraït, and S. Vieira, Phys. Rev. Lett. **76**, 2302 (1996).

⁵⁹ S. P. McGlynn, L. G. Vanquickenbourne, M. Kinoshita and D. G. Carroll, *Introduction to Applied Quantum Chemistry*, ch. 2, ch. 3, ch. 4, Holt, Reinhart and Winston Inc., 1st edn. (1972).

⁶⁰ M. Wolfsberg, L. Helmholtz, J. Chem. Phys. **20**, 837 (1952).

⁶¹ It should be noted that because the orbital basis is non-orthogonal, if the diagonal matrix elements of the bulk tight-binding Hamiltonian of Ref. 36 are shifted by *c* the non-diagonal elements must be shifted by *cS_{i,j}* for consistency.⁵⁶

⁶² The transmission away from the Fermi energy for the spin *up* configuration with this parameterization is in good qualitative agreement with that found utilizing the bulk parameters for the tip-tip coupling. The spin *down* and anti-parallel configurations also yield transmission in qualitative agreement near and away from the Fermi energy. This scheme succeeds in fitting the total transmission, and independently, the portion of the transmission due to *d* orbital coupling, and the combined transmission due to *s* and *p* orbitals, however the resulting transmission has less *p* character than for the bulk parameterization.

⁶³ The Gaussian 03 package (Revision B.05, Gaussian Inc. Pittsburgh PA, 2003) was used with the B3PW91 density functional and the Lanl2DZ basis set.

⁶⁴ Note that our use of bulk geometries and electronic parameters for the atoms of the clusters other than the tip atoms is justified by the fact that the Fe clusters in our model represent the ends of macroscopic bulk Fe leads.

⁶⁵ A similar eigenstate with enhanced weight on the tip atom of the source contact is also found but under most conditions its energy is outside of the range between the source and drain electrochemical potentials so that it does not contribute significantly to the current.